Unsteady one-dimensional model for a bed combustion of solid fuels

Won Yang[1], **Changkook Ryu**[2] and **Sangmin Choi**[1]*
[1]Department of Mechanical Engineering, Korea Advanced Institute of Science and Technology, Daejeon, South Korea
[2]Sheffield University Waste Incineration Centre, Department of Chemical and Process Engineering, The University of Sheffield, Sheffield, UK

Abstract: A transient one-dimensional combustion model of a solid fuel bed that can be applied to various types of combustors employing the solid bed is suggested. Configuration of solid beds can be characterized by combinations of solid and gas flow directions, ignition methods, and dominant reactions. These features can be reflected numerically to the boundary and initial conditions of the model, while the governing mechanism in each type of bed is similar. The mechanism is expressed as forms of conservation equations for the solid and the gas phase. Solid–gas reactions, gaseous reactions, heat transfer, geometrical changes of the particles, and physical properties are modelled and reflected to each term of the governing equations. Simulation results are shown for two cases: a packed bed combustor and an iron ore sintering bed. Two cases have distinctively different bed configurations and ignition methods. The propagation rates of the combustion zone are quantitatively discussed in terms of the flame propagation speed. Future development of the model is discussed for possible application to more complicated simulation cases.

Keywords: modelling, bed combustion, solid fuel, packed bed combustor, iron ore sintering bed

NOTATION

a	constant
A	volumetric surface area (m^2/m^3); pre-exponential factor (s^{-1})
b	constant
C	molar concentration ($kmol/m^3$)
d_p	particle size (m)
E	activation energy (J/kmol)
f_{shrink}	shrink factor
f_{ip}	ratio of internal pore generation
h	enthalpy, (J); convection coefficient (W/m^2K)
H	heat of reaction or combustion (J/kmol)
I^+, I^-	radiation intensity upward or downward (W/m^2sr)
k	rate constant (s^{-1}); conductivity (W/mK); mass transfer coefficient (m/s)
m	mass fraction; exponent
$\dot{M}$	volumetric mass generation rate (kg/m^3s)
n	bed shrinkage factor; exponent
n_p	particle number density ($1/m^3$)
p	pressure (N/m^2)
q	volumetric heat generation rate (J/m^3s)
r	reaction rate ($kmol/m^3s$)
R	universal gas constant
t	time (s)
T	temperature (K)
v	superficial velocity (m/s)
V	volume (m^3)
W	molecular weight (kg/kmol)
y	vertical coordinate (m)
α	fraction of reaction heat provided to solid particle for each reaction
β	reacting to non-reacting solid-to-gas heat transfer ratio
ε	bed void fraction, internal pore
ζ	particle area factor
κ	absorption coefficient
ν	stoichiometric coefficient density
ρ	density (kg/m^3)
τ	optical thickness

Subscripts

b	blackbody
eff	effective
g	gas

The MS was received on 9 December 2002 and was accepted after revision for publication on 23 June 2004.

**Corresponding author: Department of Mechanical Engineering, Korea Advanced Institute of Science and Technology, 373-1 Guseong-dong, Yuseong-gu, Taejon 305-701, South Korea.*

i, j	index number of solid component and gas species
k	index number of reactions
ip	internal pore
o	initial
r	Arrhenius reaction rate
s	solid, stoichiometric
u	unreacted

1 INTRODUCTION

Combustion of solid fuel as a form of bed is one of the common processes in industrial applications. The process contains complicated modes of heat and mass transfer, geometrical changes of the solid particles and bed structure, and gaseous reactions, as well as solid fuel combustion and gasification. Investigation of governing mechanisms in the process has been of great interest in connection with air pollution, as well as the combustion efficiency of the process. Numerical modelling can produce a step forward in understanding the process for design and setting operating conditions.

Extensive studies have been carried out on the numerical modelling of the process, which has various forms depending on the configurations of combustors. A one-dimensional model of coal gasifiers, which are usually co-current and/or counter-current, is one of the typical cases [**1**–**5**]. Modelling of combustion and gasification of biomass and solid waste has been reported recently [**6**–**12**]. They were also modelled as an unsteady one-dimensional system, which can be extended to a steady two-dimensional system, based on the assumption that heat and mass transfer in the vertical direction is dominant. By this method, combustion in moving beds such as waste incinerators [**9**–**12**] and iron ore sintering beds was modelled [**13**–**17**]. These models have been developed using many types of modelling reaction mechanisms and heat transfer such as radiation or flame propagation in porous media. The advanced submodels for each type of bed have enough potential to be applied to beds with different configurations, because the governing equations and basic combustion procedures have much in common. This can be achieved by a generalized modelling approach to the solid fuel beds, which has received little attention to date.

This study presents an unsteady one-dimensional (1D) model of fuel bed combustion, which can be applied to various bed configurations of packed and moving beds. Generalized forms of the numerical model are constructed using identical governing equations and solver. Users can define boundary conditions for the various configurations of the solid beds. The computational models for the combustion, geometric changes, and heat transfer are summarized. In particular, radiative heat transfer and geometrical changes of the solid particles are described in an improved manner. Application of the proposed model is demonstrated for the cases of a packed bed combustor and an iron ore sintering bed. Simulation results are shown as temperature distribution and combustion gas release pattern, and the future development of the model is discussed.

2 COMBUSTION PHENOMENA IN THE SOLID FUEL BED

Figure 1 shows the basic phenomena of a solid fuel bed during combustion. Solid particles interact with the surrounding gas media through heat and mass transfer. Solid–gas reactions, which undergo three steps – evaporation of moisture, devolatilization, and char combustion/gasification – are one of the dominant phenomena that determine the combustion characteristics within the bed. Released volatiles and other gaseous combustibles are oxidized and provide a heat source to the bed. Changes of particle sizes, generation of internal pores, and bed structure are also important parameters that affect the combustion rate.

Typical configurations of solid fuel beds are shown in Fig. 2. Bed combustion is an unsteady three-dimensional (3D) phenomenon involving a number of solid particles and surrounding gas medium. However, the bed can be simplified when streams of fuel and gas are idealized as plug flows. The packed bed in Fig. 2a can be found in batch-type reactors, which can be modelled as unsteady 1D systems. The co-current and counter-current type of beds in Figs 2b and c can be found in gasifiers or direct melting furnaces, whose steady state can be simplified as steady two-dimensional (2D) systems. The moving bed on the grates shown in Fig. 2d is applied to classic coal beds on travelling grates, the waste beds in incinerators, and so on. Although this type is two-dimensional, it can be expressed as an unsteady 1D model if the heat and mass transfer in the horizontal direction is not dominant. In this case, the horizontal location of the fuel layer can be transformed from the time elapsed and the constant moving speed.

These fuel beds have common physical and chemical mechanisms, but differ in the boundary conditions. Based on this concept, a wide range of bed combustions can be predicted from a generalized model that can treat various boundary conditions.

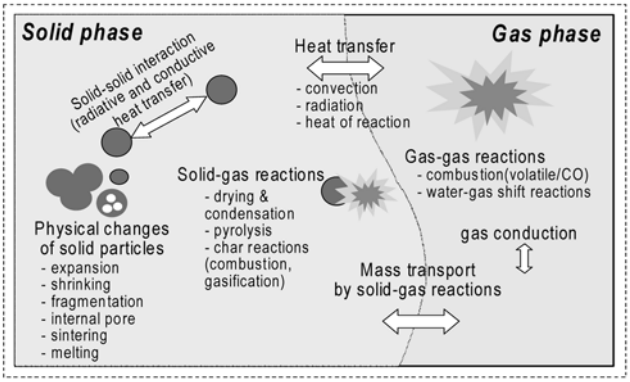

Fig. 1 Major phenomena in the solid fuel bed

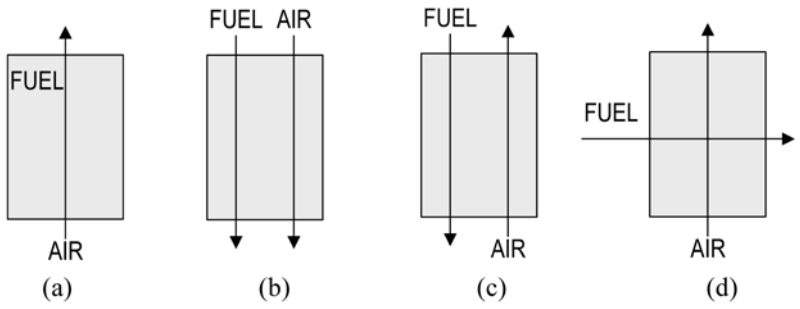

Fig. 2 Various configurations of the solid fuel bed: (a) unsteady packed, (b) steady co-current, (c) steady counter-current, and (d) cross-current moving beds

3 COMPUTATIONAL MODELLING

3.1 Modelling approach and governing equations

Fuel particles in the bed undergo unsteady 3D phenomena including interaction with the surrounding gas phase. The first step of modelling is to assume that the bed is a homogeneous continuum of the solid and gas phases in which their volume fractions are represented by the porosity, ε. For a 1D system of the y-coordinate, the governing equations are given as follows.

Solid phase:

$$\text{Mass: } \frac{\partial \rho_s(1-\varepsilon)}{\partial t} + \frac{\partial \rho_s v_s}{\partial y} = -\dot{M}_{s\to g} \tag{1}$$

$$\text{Energy: } \frac{\partial (1-\varepsilon)h_s}{\partial t} + \frac{\partial v_s h_s}{\partial y} = \frac{\partial}{\partial y}\left[(1-\varepsilon)k_s \frac{\partial T_s}{\partial y}\right] + \beta h_{conv} A_s (T_g - T_s) + q_{rad} + \alpha \dot{M}_{s-g}\Delta H_r - \dot{M}_{s-g} C_{p,s-g} T_s \tag{2}$$

$$\text{Component: } \frac{\partial \rho_s(1-\varepsilon)m_{s,i}}{\partial t} + \frac{\partial \rho v_s m_{s,i}}{\partial y} = \dot{M}_{s,i} \tag{3}$$

Gas phase:

$$\text{Mass: } \frac{\partial \rho_g \varepsilon}{\partial t} + \frac{\partial \rho_g v_g}{\partial y} = \dot{M}_{s\to g} \tag{4}$$

$$\text{Energy: } \frac{\partial \varepsilon_v h_g}{\partial t} + \frac{\partial v_g h_g}{\partial y} = \frac{\partial}{\partial y}\left(\varepsilon k_g \frac{\partial T_g}{\partial y}\right) + \beta h_{conv} A_{po}(T_s - T_g) + (1-\alpha)\dot{M}_{s-g}\Delta H_r + \dot{M}_{s-g} C_{p,s-g} T_s \tag{5}$$

$$\text{Chemical species: } \frac{\partial \rho_g \varepsilon m_{g,j}}{\partial t} + \frac{\partial \rho_g v_g m_{g,j}}{\partial y} = \dot{M}_{g,j} + \dot{M}_{s\to g,j} \tag{6}$$

$$\text{Equation of state: } \rho_g = p/R \sum \frac{m_j}{W_j} T_g \tag{7}$$

where the velocity, v, is a Darcean or superficial velocity. The heat and mass interaction of the two phases, as well as the chemical changes in each phase, are incorporated in the source term S_ϕ. The pressure drop in the gas phase by the solid particles was neglected for simplicity.

3.2 Solid fuel combustion

Combustion of solid fuels is typically classified into three distinctively different steps: moisture evaporation, pyrolysis, and char combustion/gasification. In each process, reactants as well as products include both solid and gaseous species. Equations of reaction can be expressed in a generalized form as shown below.

$$\sum_{\text{solid}} v_i' M_i + \sum_{\text{gas}} v_j' M_j \longrightarrow \sum_{\text{solid}} v_i'' M_i + \sum_{\text{gas}} v_j'' M_j \tag{8}$$

The moisture evaporation should be considered in two ways: boiling and diffusion below the boiling temperature. Upon contact with the cold surface, evaporated vapour may recondense.

$$r_{\text{drying@373 K}} = \frac{\sum q_{in}}{\Delta H_{drying}\Delta t} \tag{9a}$$

$$r_{\text{drying}<373\text{ K}} = A_s k_{m,H_2O}(C_{\text{moisture,sat}} - C_{g,H_2O}) \tag{9b}$$

The reaction rates of the pyrolysis and char combustion are determined from the kinetic rate, diffusion rate, and the internal mass transport in the ash layer of the particle [**2**]. The kinetic rate is controlled by particle area factor, ζ

$$k_{\text{pyrolysis}} = \left(\frac{1}{k_r} + \frac{1}{k_m} + \frac{1}{k_{\text{eff}}}\right)^{-1} \tag{10}$$

$$r_{\text{char}} = A_s v_s C_{g,\text{oxidant}} d_p \Big/ \left(\frac{1}{k_r \zeta} + \frac{1}{k_m} + \frac{1}{k_{\text{eff}}}\right) \tag{11}$$

3.3 Geometric properties

Solid fuel combustion causes volumetric reduction, generation of internal pores, or both. The fraction of conversion to the internal pores is expressed with a factor, f_{ip}, for each solid component. From this factor and from the combustion rate, the particle size and the internal porosity are determined. The changes in the particle size are described

by the well-known shell progressive (SP) and ash segregation (AS) models [**2**]. Then, the number density and the volumetric surface area of the particles are derived from the porosity and the particle size.

$$n_{\mathrm{p}} = \frac{6(1-\varepsilon)}{\pi d_p^3}, \qquad A_{\mathrm{s}} = \pi d_{\mathrm{p}}^2 n_{\mathrm{p}} \tag{12}$$

The porosity is a packing property of the bed material and is calculated from the volumetric shrinkage of the particle. It can be expressed in the general form by introducing a packing parameter n as,

$$(1-\varepsilon) = f_{\mathrm{s}}^{1-n}(1-\varepsilon_{\mathrm{o}}) \qquad \text{where}$$
$$f_{\mathrm{shrink}} = \frac{V_{\mathrm{p}}}{V_{\mathrm{p,o}}} = \left(\frac{d_{\mathrm{p}}}{d_{\mathrm{p,o}}}\right)^3 \tag{13}$$

If the exponent n is a unity, the porosity does not change. Then, the particle shrinkage results in changes in the particle number density and, subsequently, the bed height. If it is zero, then the shrinkage leads to an increase in porosity. Thus, the density and the bed height do not change.

On the other hand, generation of the internal pore within the particles is represented by the internal porosity, which is defined as

$$\varepsilon_{\mathrm{ip}} \equiv \frac{V_{\mathrm{ip}}}{V_{\mathrm{s}}} = 1 - \frac{V_{\mathrm{s,true}}}{V_{\mathrm{s}}} = 1 - \frac{\rho_{\mathrm{s}}}{\rho_{\mathrm{s,true}}} \tag{14}$$

Thus, the density of the solid phase is determined from the internal porosity and the true density of the solid components.

$$\rho_{\mathrm{s}} = (1-\varepsilon_{\mathrm{ip}})\rho_{\mathrm{s,true}} \qquad \text{where}$$
$$1/\rho_{\mathrm{s,true}} = \sum_i m_{\mathrm{s},i}/\rho_{\mathrm{s},i} \tag{15}$$

Describing the internal porosity requires a transport equation, since the internal pore moves along through the advection of the solid phase, expressed as given below.

$$\frac{\partial(1-\varepsilon)\varepsilon_{\mathrm{ip}}}{\partial t} + \frac{\partial v_{\mathrm{s}}\varepsilon_{\mathrm{ip}}}{\partial y} = -\sum_i f_{\mathrm{ip},i}\frac{\dot{M}_{\mathrm{s},i}}{\rho_i} + \dot{\varepsilon}_{\mathrm{ip,loss}} \tag{16}$$

The first source term in the right-hand side indicates the generation of the internal pore by the contribution ($f_{\mathrm{ip},i}$) of the component mass loss. The second term is its loss by ash segregation, if activated. This equation is solved numerically by a method identical to the governing equations.

3.4 Gaseous reactions

Gaseous reactions occur within the bed by the combustible products of pyrolysis and char combustion released from the fuel particles. The reaction scheme should be chosen according to the reactants and the reaction environment. The kinetic rate of reaction r is expressed in general form as

$$r_k = A_k \prod C_j^{n_{j,k}} T_{\mathrm{g}}^{a_k} p^{b_k} \exp(-E_k/RT_{\mathrm{g}}) \tag{17}$$

3.5 Heat and mass transfer

Dominant modes of heat transfer in the packed bed are conduction in the solid and gas phases, radiation in the solid phase, and convection. The conduction is solved as a diffusion of energy, once the conductivity is calculated. Convection in the packed bed is expressed as [**18**]

$$Nu = a + bRe^m Pr^n \tag{18}$$

Mass transfer of the gas phase is solved by an analogy with the convection.

$$Sh = a + bSc^m Pr^n \tag{19}$$

Radiation in the solid phase is solved using the two-flux method [**9**]. The scattering is neglected, which simplifies the equation significantly. The absorption coefficient is determined from the particle size and the porosity, based on the assumption that the radiation intensity decreases by a factor of e for a distance of d_{p}.

$$\frac{1}{2}\frac{\mathrm{d}I^+}{\mathrm{d}\tau} = I_b - I^+, \qquad -\frac{1}{2}\frac{\mathrm{d}I^-}{\mathrm{d}\tau} = I_b - I^- \tag{20}$$

This model can easily handle the exposure of the bed to the external radiation in a furnace enclosure as a boundary condition. The entire set of above-listed equations is solved using the Runge–Kutta method. Each cell in the radiation calculation is automatically divided into several subcells to guarantee the calculation accuracy.

4 CALCULATION CASES

The computational model can be applied to various configurations of the solid bed. A batch-type packed bed and an iron ore sintering bed were selected for the calculation cases. Figure 3 shows the schematic diagram of a batch-type packed bed of wood cubes. The bed has a diameter of 15 cm and a height of 45 cm. The bed section is inserted into a furnace maintained at 1123 K by an electric heater and, then, is ignited by radiation from the furnace wall. Combustion air is supplied from below the bed. As shown in Fig. 3b, the global combustion process follows the drying, pyrolysis, and char combustion. Pyrolysis and volatile combustion play an important role in the propagation of

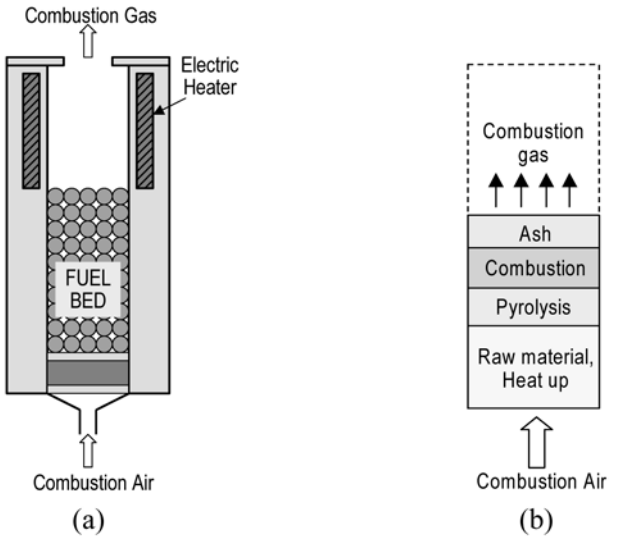

Fig. 3 Schematic diagram of the packed bed of wood cubes: (a) packed bed combustor, (b) major phenomena in the bed

the combustion zone, which is determined from the heat balance near the ignition point. Heat generated from the fuel combustion and gaseous reactions above the ignition front is transferred to the unburned fuel by radiation and conduction.

A schematic diagram of the iron ore sintering process, which has a moving bed, is shown in Fig. 4. Sintering is the agglomeration of small metal or ceramic particles by surface melting. In the iron-making process, the sintering process produces large particles (>5 mm) of iron ore with the appropriate metallurgical properties required in the blast furnace. A raw mix of iron ores and other additives including a selected amount of coke as an energy source form a bed on a travelling grate. Air is supplied to the bed by a downdraught suction fan. The combustion is initiated at the top of the bed by a hot gas jet from the ignition burners for a few minutes after the feed material is introduced into the bed, and propagates into the bed while the solid particles are sintered near the combustion front. Prevention of excessive melting is very important when the flame front reaches the bottom of the bed, since the melted ore at the bottom may plug up the grate slits, causing serious operating problems. For this purpose, a hearth bed is installed at the bottom of the bed, using previously sintered particles of

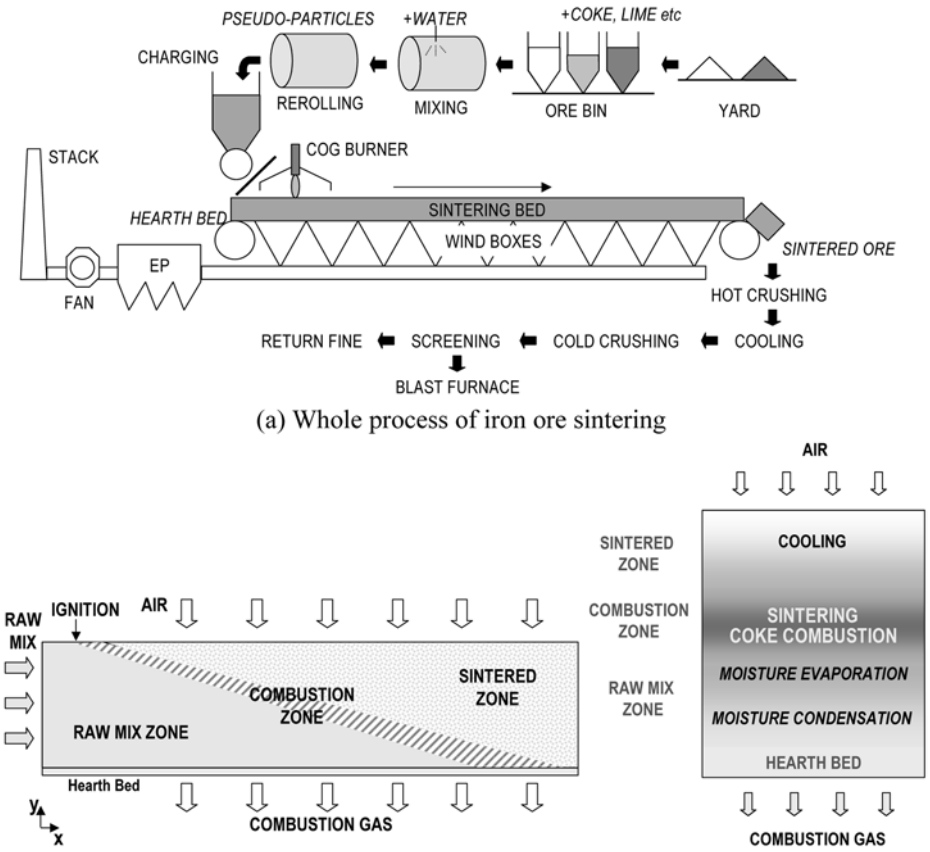

Fig. 4 Schematic diagram of an iron ore sintering process: (a) whole process of iron ore sintering, (b) major phenomena in the iron ore sintering bed

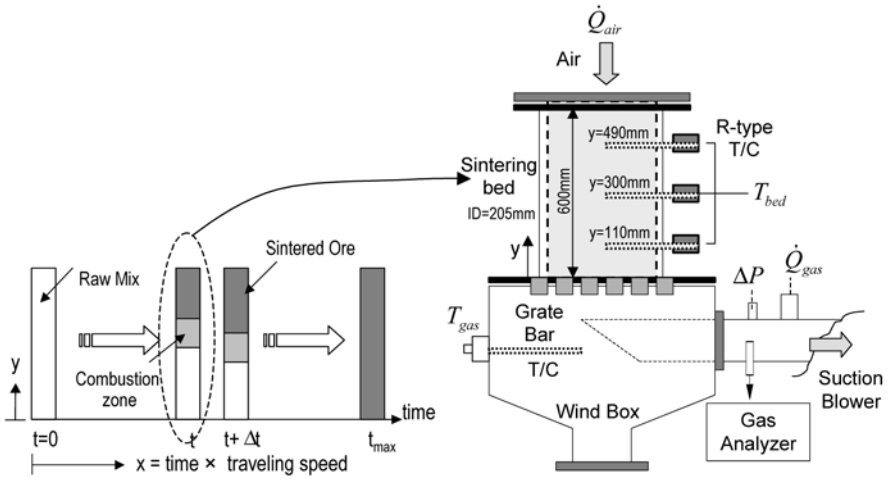

Fig. 5 Concept and schematic diagram of the sintering pot test

larger size excluding any heat source such as coke. The iron ore sintering bed has a height of ~0.6 m and a length of ~100 m in industrial applications and measurement data are very hard to obtain. Measurement data are usually obtained in a laboratory-scale sintering pot test, of which a schematic and a concept diagram is shown in Fig. 5. Because the sintering bed is a moving bed with a constant travelling speed, the distribution along the direction of length can be obtained by transforming the time using the travelling speed. The bed of the sintering pot has a height of 60 cm and an inner diameter of 20.5 cm. R-type thermocouples are installed along the height to measure the solid bed temperature. Gas flow rate and composition can be continuously monitored during the test.

Major features of the selected beds are summarized in Table 1. The packed bed combustor is a fixed bed, and the iron ore sintering bed is a moving bed, with a constant travelling speed in the horizontal direction. Each type of solid fuel bed differs in some of its characteristics such as the type of fuel, ignition method, and the mechanism of the physical changes of the solid particles. They were reflected in the boundary and/or initial conditions.

Table 2 summarizes major input conditions and model parameters of the packed bed combustor and the iron ore sintering bed. For the packed bed combustor, the bed material is assumed to be homogeneous particles of 20 mm diameter. Pyrolysis and char combustion are considered as major solid–gas reactions. Volatile combustion and water–gas shift reactions are taken into account for calculating gaseous reactions. Volatiles and char components are considered as the single hypothetical hydrocarbon, $C_xH_yO_z$. As for the iron ore sintering bed, the iron ores and limestone are assumed to be chemically inert material, which implies that the reduction of iron ores and limestone decompositions

Table 1 Major characteristics of types of solid fuel beds

	Packed bed combustor	Iron ore sintering bed
Bed type	Fixed bed	Moving bed
Bed material	Wood cubes	Iron ore + Limestone + Coke
Feeding	Batch	Continuous
Ignition method	Radiation	Gas burner
Behaviour of inert material in the solid	Not important	Important

Table 2 Major input conditions and model parameters for the packed bed combustor and the iron ore sintering bed

	PBC	IOSB
Bed height (m)	0.45	0.62
No. of cells	100	40
t_{max} (s)	6000	1800
Δt (s)	1	1
Fuel		
Size	20 mm	3 mm
Moisture	25%	6.5%
Volatile	55%	0.0%
Char	10%	3.8%
Ash	10%	89.7%
ε_o	0.54	0.4
LHV	2374	—
f_{ip}	0 (char) 1 (else)	0 (all)
Oxidizer		
Type	Air	Air
T	300 K	300 K
v	0.05 m/s	0.35 m/s
Ignition		
Type	Radiation	Hot gas (4 m/s)
Temp.	850 K	1403 K
Time	Whole process	90 s
Pyrolsis		
A	1.5×10^4	Not considered
E	30 kcal/kmol	Not considered
Char reactions		
A	2.3	2.3
E	22 kcal/kmol	22 kcal/kmol
Gaseous reactions	$Volatile + O_2 \rightarrow CO + H_2$ $CO + H_2O \leftrightarrow CO_2 + H_2$ $H_2 + 0.5O_2 \rightarrow H_2O$ Rate [9]	$CO + 0.5O_2 \rightarrow CO_2$ $H_2 + 0.5O_2 \rightarrow H_2O$ Rate [9]

PBC, packed bed combustor; IOSB, iron ore sintering bed; LHV, lower heating value (kcal/kg). A, pre-exponential factor; E, activation energy.

Table 3 Assumed model parameters that cannot be measured

	Fixed bed gasifier	Iron ore sintering bed
α^*	0.6	0.6
β^*	1	0.1 [**2**]
ζ^*	0.5 [**9**]	0.1 [**2**]
n^*	1	1

*See notation list.

are not considered. We do not address sintering itself in this study either, because it would require specific metallurgical models that describe the rate of sintering and corresponding changes in the particle size and porosity. Validation of the model for the sintering bed is attempted using the results from the reduced-scaled sintering pot tests. Measurement results can be shown by transforming the time axis to the directions of a constant-speed moving grate, which gives the impression of real-scale sintering beds.

Additionally, there are some model parameters that cannot be measured, but must be selected from previous researchers' works [**2**, **9**]. The parameters are summarized in Table 3.

5 RESULTS AND DISCUSSION

Figure 6 shows the measurement and computational results for the packed bed combustor. First, the top of the bed is ignited by radiation from the electric heater. Each solid fuel particle undergoes complicated combustion processes: drying, pyrolysis, and char combustion. Dry wood is composed of 84.6 per cent volatile, 15.3 per cent fixed carbon, and a very small amount of ash. Therefore, pyrolysis and volatile combustion play a key role in the propagation of the combustion zone, and they are dominant reactions in the bed. Therefore, thermal diffusivity in the bed is larger than

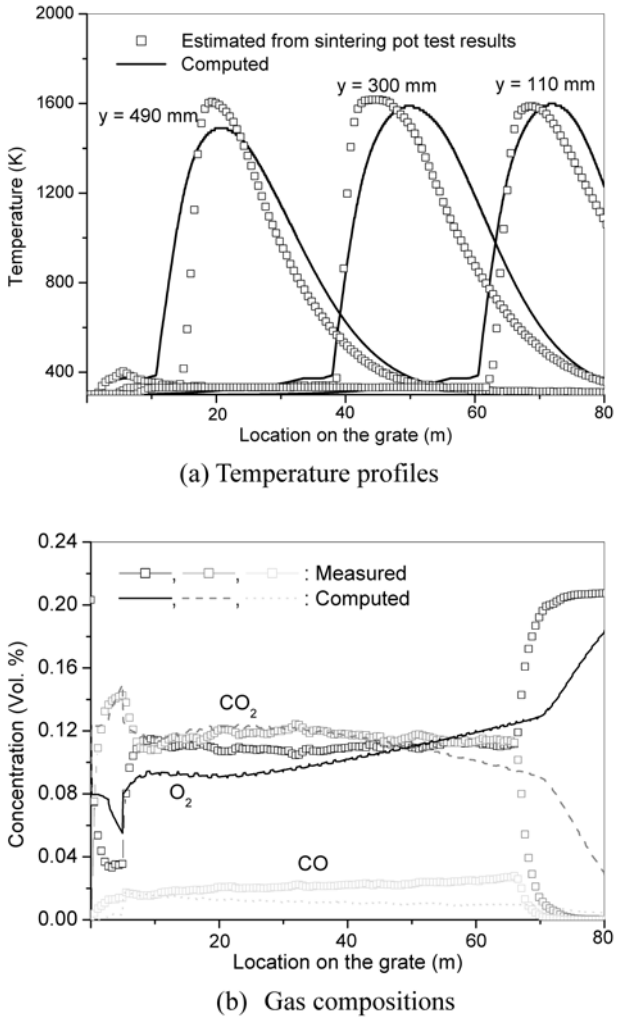

Fig. 7 Simulation results of the iron ore sintering bed with experimental results: (a) temperature profiles, (b) gas compositions

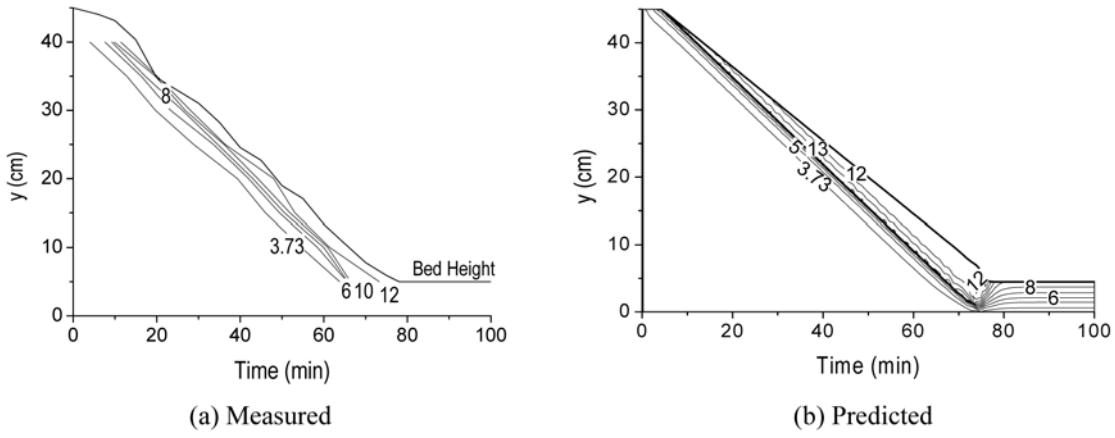

Fig. 6 Measured and predicted temperature distributions (×100 K) for the packed bed of wood cubes: (a) measured results, (b) predicted results

in an iron ore sintering bed, which can have maximum temperature of ~1700 K [**15**–**17**]. It is well established that the maximum temperature of the wood bed does not exceed ~1200 K. The size of solid particles is dramatically decreased during the combustion process, which causes a decrease in bed height. The thickness of the combustion zone is small (<5 cm) because most of the solid material is combustible. The remaining material, which has a height of ~6 cm in the bed after the whole combustion process, is inert material that was previously positioned to support the particle bed. Simulation results show a good agreement with the experimental data [**9**], which implies that the model reasonably predicts the heat transfer, including the fuel combustion and gaseous reaction that determines the combustion zone thickness and the propagation speed of the combustion front.

Figure 7 shows the solid temperature profiles and gas compositions within the iron ore sintering bed. As the coke combustion zone progresses downward, the solid temperature at a certain point begins to rise and sustains for the period where the fuel component remains. After reaching the peak, the temperature gradually drops to room temperature, by balancing the heat generation and convection cooling from the inlet air. The simulation results were compared with the estimated experimental data from the laboratory-scale sintering pot tests. The simulation results show general agreement with the experimental results, although there are some differences in the temperature profiles at y = 490 mm and gas compositions after the bed proceeds 70 m for the location on the grate.

Figure 8 shows the solid temperature distribution within the bed for various air inlet velocities. As the combustion propagates into the bed, the higher temperature region becomes larger by convection from the combustion gas. For lower air velocity, the combustion zone propagates slowly and the temperature is lower than that of the reference case. The amount of oxygen significantly influences the combustion rate in these cases. However, as inlet air velocity exceeds a certain amount, the combustion zone becomes thinner and the temperature is lower than the reference case due to the convection heat loss. Finally, combustion cannot be self-sustained when the air inlet velocity increases further. Similar results were reported for the case of a batch-type packed bed combustor [**9**].

Quantification of the calculation results can be performed by introducing the flame front speed (FFS), which can be defined as [**9**]

$$\text{FFS (cm/min)} = \frac{\text{Distance between two points @ 1000 K}}{\text{Time consumed for propagation}} \tag{21}$$

Figure 9 shows the FFS values for air velocities for the iron ore sintering bed. From previous researchers' work, the graph

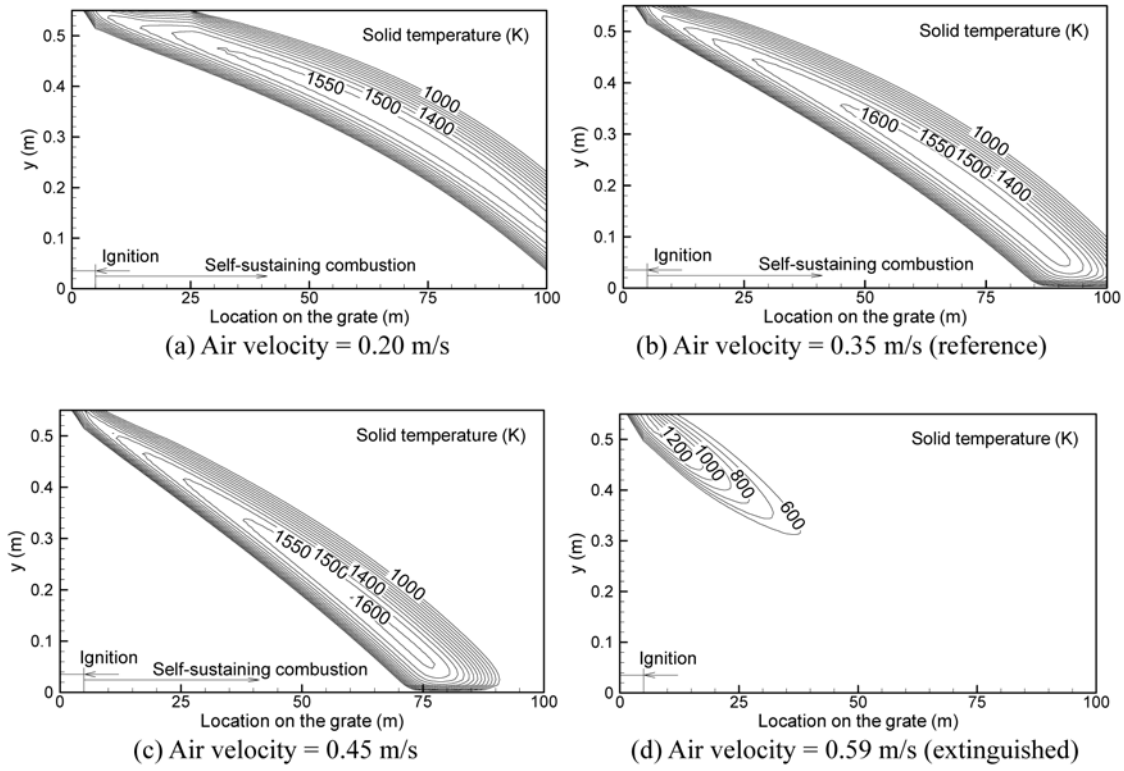

Fig. 8 Temperature distributions (×100 K) of the solid phase for various air inlet velocities in the iron ore sintering bed: air velocity of 0.20 m/s, (b) 0.35 m/s (reference), (c) 0.45 m/s, and (d) 0.59 m/s (extinguished)

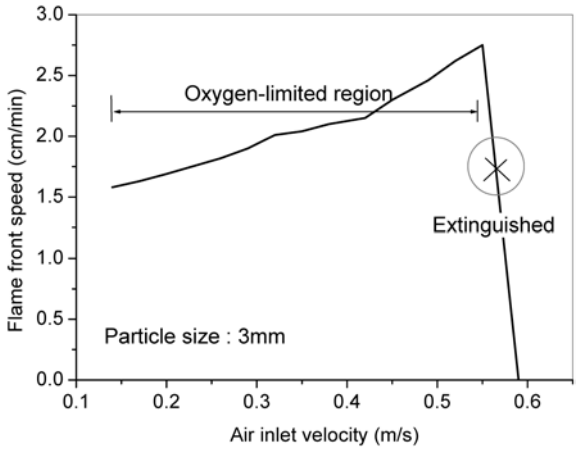

Fig. 9 Flame front speed (FFS) for various air velocities

should be divided into three regions: oxygen-limited region, diffusion-limited region, and the region in which flame becomes extinct [**9**]. In the oxygen-limited region, the FFS is dominated by the oxygen supply, but it is dominated by oxygen diffusion in the diffusion-limited region. The combustion front becomes extinct by excessive convection cooling when the air velocity exceeds the limiting value. However, the FFS curve shown in Fig. 9 does not show the diffusion-limited region, where FFS is independent of the air supply rate. This is due to the fact that the particle size in the sintering bed is much smaller (typically 3 mm in diameter) than the one used in the fixed bed experiment (typically 20 mm in diameter) [**8**].

The model suggested in this study shows good agreement with the experimental results for the cases of a packed bed and a moving bed where the solid and gas streams can be simplified as plug flows. However, this model can be extended further, from a generalized modelling point of view. First, the model could incorporate a particle resolved approach from single particle combustion models to predict the temperature distribution and corresponding co-existence of combustion processes. Each particle is divided into several shells, and the outer shell has convection with the surrounding gas media, while the inner shells only have conduction with nearby ones. Secondly, the bed structural changes during the combustion, which would induce change of the porosity, should also be considered in the current model. Change of the porosity would affect the pressure drop across the solid bed, which significantly influences the air supply rate. Finally, extension of the current model to 2D cases would improve the utility of the model, especially for moving beds. Heat and mass transfer in the traverse direction have to be considered. Mixing of the solid particles by moving grates could be accounted for by virtual diffusion or a momentum source.

6 CONCLUSIONS

An unsteady 1D model was proposed for the bed combustion of solid fuels, based on the assumption of a homogeneous solid fuel bed and the plug flow of the solid and gas streams. The model can consider various bed configurations and ignition methods by flexibly employing the boundary conditions. Because fuel combustion, gaseous reaction, and geometric changes in the fuel beds are based on the common governing mechanism, numerical models were constructed in a generalized form that can be applied to the various application systems. Simulation results of this model were shown for the cases of the batch-type packed bed and an iron ore sintering bed. The predicted temperature distribution and the flame propagation pattern show the validity and applicability of the model. Bed structural changes and model extension to two dimensions should be considered in future studies.

ACKNOWLEDGEMENTS

The presented work was financially supported by POSCO and was a part of the programme of International Collaborative Research financially supported by the Korea Ministry of Science and Technology.

REFERENCES

1 **Goldman, J., Xieu, D., Oko, A., Raymond, L.** and **Essenhigh, R. H.** A comparison of prediction and experiment in the gas gasification of anthracite in air and oxygen-enriched/steam mixtures. *12th Symposium (International) on Combustion/The Combustion Institute*, Ann Arbor, USA, 1984, pp. 1365–1372.
2 **Hobbs, M. L., Radulovic, P. T.** and **Smoot, L. D.** Modeling fixed-bed coal gasifiers. *AIChE J.*, 1992, **38**(5), 681–702.
3 **Radulovic, P. T., Ghani, M. U.** and **Smoot, L. D.** An improved model for fixed bed coal combustion and gasification. *Fuel*, 1995, **74**(4), 582–594.
4 **Cooper, J.** and **Hallett, W. L. H.** A numerical model for packed-bed combustion of char particles. *Chem. Eng. Sci.*, 2000, **55**, 4451–4460.
5 **Smoot, D.** *Fundamentals of Coal Combustion in Coal Science and Technology*, 1993, pp. 630–673 (Elsevier Science Publishers, Amsterdam).
6 **Kuo, J. T.** Estimation of burning rates in solid waste combustion furnace. *ASME National Waste Processing Conference*, Detroit, Michigan, 1994, 177–183.
7 **Goh, Y. R., Siddall, R. G., Nasserzaheh, V., Zakaria, R., Swithenbank, J., Lawrence, D., Garrod, N.** and **Jones, B**. Mathematical modeling of the burning bed of a waste incinerator. *J. I. Energy*, 1998, **71**, 110–118.
8 **Oman, J., Tacer, M.** and **Tuma, M.** Overfed fixed-bed combustion of wood. *Biores. Technol.* 1999, **67**(2), 139–147.
9 **Shin, D.** and **Choi, S.** The combustion of simulated waste particles in a fixed bed. *Combust. Flame*, 2000, **121**, 167–180.
10 **Blasi, C. D.** Dynamic behaviour of stratified downdraft gasifiers. *Chem. Eng. Sci.*, 2000, **55**, 2931–2944.
11 **Wurzenberger, J. C., Wallner, S. W., Raupenstrauch, H.** and **Khinast, J. G.** Thermal conversion of biomass: Comprehensive reactor and particle modeling. *AIChE J.*, 2002, **48**, 2398–2411.

12 **Ryu, C., Shin, D.** and **Choi, S.** Combined bed combustion and gas flow simulation for a grate type incinerator. *J. Air Waste Manage.*, 2002, **52**(2), 189–197.
13 **Muchi, I.** and **Higuchi, J.** Theoretical analysis on the operation of sintering. *Testu-to-Hagane*, 1970, **56**(3), 371–381.
14 **Hosotani, Y., Fujimoto, M., Konno, N., Okada, T.** and **Shibata, J.** Influence of oxygen and humidity of inlet gas on the sintering reaction. *Testu-to-Hagane*, 1997, **83**(5), 7–12.
15 **Ramos, M. V., Kasai, E., Kano, J.** and **Nakamura, T.** Numerical simulation model of the iron ore sintering process directly describing the agglomeration phenomenon of granules in the packed bed. *ISIJ Int.*, 2000, **40**(5), 448–454.
16 **Patisson, F., Bellot, J. P., Ablitzer, D., Marliere, E., Dulcy, C.** and **Steiler, J. M.** Mathematical modelling of iron ore sintering process. *Ironmak. Steelmak.*, 1991, **18**(2), 89–95.
17 **Nath, N., Da Silva, J.** and **Chakraborti, N.** Dynamic process modelling of iron ore sintering. *Steel Res.*, 1997, **68**(7), 285–292.
18 **Wakao, N.** and **Kaguei, S.** *Heat and Mass Transfer in Packed Beds*, 1982 (Gordon and Breach, New York).
19 **Patankar, S. V.** *Numerical Heat Transfer and Fluid Flow*, Series in Computational Methods in Mechanics and Thermal Sciences, 1980, pp. 58–59 (Hemisphere, USA).